Journal of Progress in Engineering and Physical Science
ISSN 2709-4006
www.paradigmpress.org/jpeps
Volume 5 Number 3 September 2026

Residual Coal-Fire Evidence After Control Operations in a Mining Critical Zone, Inner Mongolia, China

Jiahao Liu[1,2], Shitao Zhang[3], Rong He[3], Xiongfei Zhang[3], Yao Xiang[2]

[1] Marist Brothers International School, Beijing 100103, China
[2] School of Chemical Sciences, University of Chinese Academy of Sciences, Beijing, China
[3] Inner Mongolia Taixi Coal Group Co., Ltd., Alxa Left Banner, Inner Mongolia 750306, China
Correspondence: Xiongfei Zhang, Inner Mongolia Taixi Coal Group Co., Ltd., Alxa Left Banner, Inner Mongolia 750306, China; Yao Xiang, School of Chemical Sciences, University of Chinese Academy of Sciences, Beijing, China.

doi:10.63593/JPEPS.2026.09.04

Abstract

A reduction in mapped surface fire area is commonly interpreted as evidence of coal-fire control, but it does not necessarily reflect the state of a three-dimensional subsurface combustion system. Here, we analyze field measurements and survey products collected during investigations conducted in 2021 and January 2024 in the Erdaoling mining area of the Gulangben coalfield, Inner Mongolia, China. The 2024 survey covered approximately 10.63 km² and integrated UAV thermal-infrared imagery, UAV-derived orthophotography, ground observations, DInSAR deformation data, and borehole measurements. A total of 71 high-temperature anomalies were identified, including 44 fire-zone units covering 81,252.80 m² and 27 high-temperature gangue-pile units covering 95,957.27 m². The 2021 investigation reported a mapped fire area of 83,241 m²; however, differences in survey extent and anomaly-classification procedures preclude a formal estimate of fire-area decay. Field observations documented fire-zone surface temperatures of 40–165 °C, flame temperatures of 630-800 °C, borehole temperatures of approximately 64.6-82.5 °C, and CO concentrations of approximately 276-1000 ppm at selected boreholes. Two open-fire points exceeding 380 °C were also identified in 2024. Fire-zone units were spatially associated with steeply dipping coal seams, mined ground, goafs, and fractured zones, indicating that geological conditions and mining disturbance jointly define the spatial context of residual combustion, although the relative contribution of individual structural factors remains unresolved. The results demonstrate that fire-zone delineation, hot-gangue-pile identification, field temperature and gas observations, borehole anomalies, and DInSAR deformation provide complementary but non-equivalent evidence. A reduction in mapped surface fire area alone is therefore insufficient to verify subsurface fire extinction.

Keywords: UAV thermal infrared, DInSAR, post-remediation monitoring, gangue pile, carbon monoxide

1. Introduction

Underground coal fires are persistent environmental and geohazard sources. They

consume coal resources, release carbon-containing and toxic gases, alter ground stability, degrade soil and vegetation, and complicate subsequent mining and fire-control operations (Claudia Kuenzer & Stracher, 2012; Claudia Kuenzer et al., 2007; Liang, Yang, Guo, Tian, & Wang, 2023a; Song & Kuenzer, 2014; Stracher & Taylor, 2004; Tao Wang et al., 2023). Their persistence reflects the interaction of low-temperature oxidation, heat accumulation, oxygen access, seam geometry, abandoned workings, and fracture-controlled transport (Liang, Yang, Guo, Tian, & Wang, 2023b; Lu et al., 2022). In steeply dipping coalfields, a surface intervention can remove or cover shallow burning material while leaving deeper heat sources, voids, and gas pathways. The disappearance of a flame or the reduction of a mapped surface anomaly is therefore an operational observation rather than a complete proof of underground extinction. Previous studies have established several tools for investigating this problem. Laboratory and field research has clarified the temperature-dependent oxidation of coal and the production of CO and CO_2 during self-heating (Carras, Day, Saghafi, & Williams, 2009; Carras & Young, 1994; Li et al., 2020; Moshood Onifade, 2022; M. Onifade & Genc, 2020; Song, Huang, Jiang, & Pan, 2020; Y. Zhang et al., 2015; Zhou et al., 2017). Studies of goafs and underground fire systems have emphasized the role of air leakage, porous pathways, abandoned workings, and chimney-like flow in sustaining combustion (Liang et al., 2023a; Song, Huang, Kuenzer, et al., 2020). Satellite and airborne thermal infrared data provide regional detection of surface heat, while unmanned aerial vehicle (UAV) systems can resolve fragmented fire points, hot ground, cracks, and waste piles at finer spatial scales (Shao, Li, Deng, Wang, & Zhong, 2021; Turner, Lucieer, Malenovský, King, & Robinson, 2014; X. Zhang, Zhang, Kuenzer, Voigt, & Wagner, 2004). Differential interferometric synthetic aperture radar (DInSAR) adds information on surface deformation associated with mining disturbance and subsurface changes (Raju & Mehdi, 2023; Teng Wang et al., 2022). These methods are complementary, but they observe different parts of the fire system. Thermal imagery measures a surface expression, gas records are often point-based, boreholes provide sparse depth constraints, and deformation records depend on the observation period and surface coherence (Agarwal, Singh, Chauhan, & Singh, 2006; Chatterjee, 2006; C. Kuenzer, Hecker, Zhang, Wessling, & Wagner, 2008; C. Kuenzer et al., 2007; Prakash & Gupta, 1999).

Several unresolved problems follow from this difference in observation scale. First, many fire studies compare surface thermal areas across dates without a complete audit of survey boundaries, classification rules, and spatial registration. This can turn methodological differences into an apparent fire trend. Second, surface thermal maps are often not co-registered with repeated field temperature, gas, and borehole observations, which limits the ability to distinguish an active coal seam from a hot waste pile or a shallow heated surface. Third, CO, CO_2, O_2, and CH_4 are rarely available as synchronized measurements at the same locations and times in long-term field investigations, so laboratory oxidation stages cannot be transferred directly to complex mine sites. Fourth, a single or short-period deformation product cannot resolve whether a weak surface deformation signal reflects cooling, rigid overburden, spatial separation, or a limited observation window. These limitations make it difficult to determine whether a shrinking surface footprint represents true subsurface decay, spatial redistribution of residual heat, or a change in the detectable surface expression (Carras et al., 2009; Carras & Young, 1994; C. Kuenzer, Bachmann, Mueller, Lieckfeld, & Wagner, 2008; M. Onifade & Genc, 2020).

The Erdaoling mining area provides a data-rich field setting for examining this problem. The January 2024 field survey covered approximately 10.63 km^2 across the Biligou, Hashatu, Changgou, and Gulangben mining areas and the Daling No. 1 historical fire area. The area contains Middle to Lower Jurassic coal-bearing strata, steeply dipping seams, old workings, goafs, excavation pits, stepped slopes, waste platforms, and mapped fractures. The 2024 measurements identified 44 mapped fire-zone and 27 hot-waste-pile units, while the 2021 field program included five verification boreholes and depth-resolved temperature and CO observations. The dataset also contains dated observations from earlier field surveys and a Sentinel-1A DInSAR pair acquired between September and December 2023. These measurements do not form a fully repeated monitoring experiment, but they allow the relationships among surface thermal classes, field observations, sparse subsurface evidence,

and short-period deformation to be examined explicitly.

This study addresses one central question: can a reduction in the mapped surface thermal-fire footprint reliably indicate the attenuation of underground coal-fire activity in the Erdaoling mining area? We evaluate this question by separating fire-zone polygon, hot-waste-pile polygons, field temperature and gas observations, borehole constraints, deformation observations, and resource-loss calculations into distinct evidence classes. The analysis tests the proposition that surface thermal contraction can coexist with residual subsurface or hidden thermal evidence, that surface, subsurface, and gas indicators can be spatially decoupled, and that weak short-period DInSAR deformation cannot by itself exclude residual combustion. The study does not estimate a causal treatment effect. Instead, it uses field data collected by the authors to define what the measurements support, what they do not support, and how multi-source evidence should be combined when evaluating residual coal-fire risk.

2. Materials and Methods

The dataset analyzed in this study was generated through field investigations and monitoring conducted by the authors in 2021 and January 2024. It includes UAV thermal-infrared imagery, orthophotography, ground-temperature and gas observations, fire and hot-waste-pile polygons, borehole measurements, geophysical logging, DInSAR products, geological observations, and resource-loss calculations. The 2021 and 2024 datasets are identified by their measurement periods rather than treated as external documentary sources. For every record, we retain the measurement date, survey extent (as shown in Figure 1), measurement type, spatial identifier, and interpretation status. Values from different survey boundaries or different evidence types are not treated as directly interchangeable.

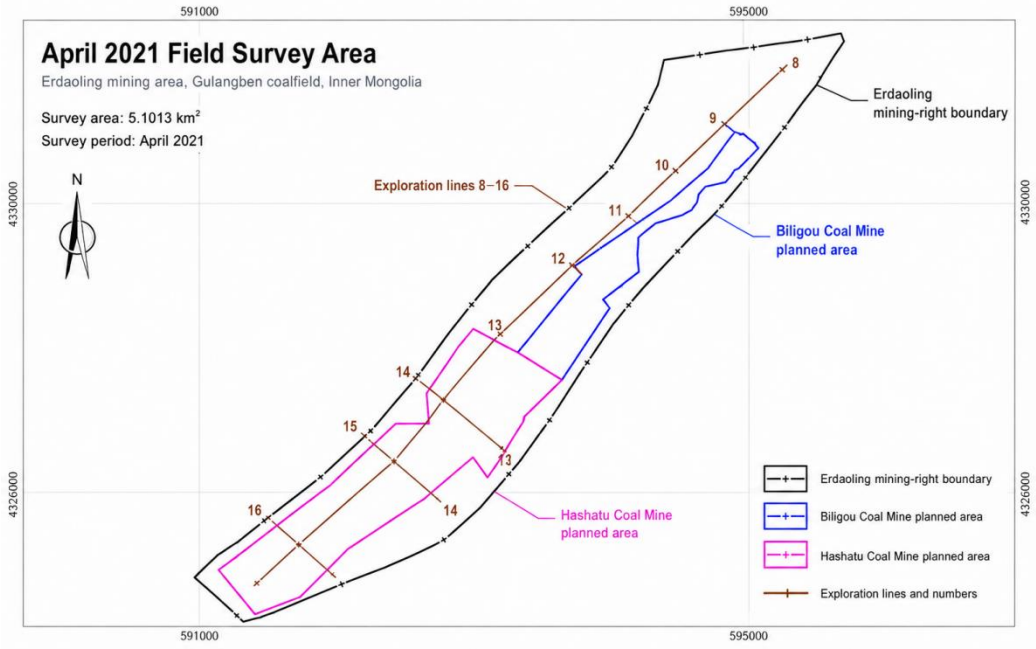


Figure 1. Spatial coverage of the January 2024 UAV survey in the Erdaoling mining area, Inner Mongolia, China. The survey covered approximately 10.63 km² across the Biligou, Hashatu, Changgou, and Gulangben sectors, with mining boundaries and exploration lines shown schematically.

2.1 Study Area and Geological Setting

The Erdaoling mining area is located in the Gulangben coalfield of Alxa Left Banner, Inner Mongolia, China. The 2021 field survey focused on the fire zone along exploration lines 8 to 16 and covered approximately 5.1013 km² in the Biligou and Hashatu sectors. The 2024 field survey expanded the mapped work area to approximately 10.63 km² and included Biligou, Hashatu, Changgou, Gulangben, the Daling No. 1 historical fire area, and adjacent mining boundaries defined during the survey. Because these two survey areas have different spatial

extents, their fire areas are compared descriptively rather than used as a formally matched time series.

The area occupies the western slope of the Helan Mountains. Ground elevation ranges from approximately 1838.3 to 2201.2 m, with a relative relief of about 362.9 m. The coal-bearing strata belong mainly to the Middle to Lower Jurassic Yan'an Formation. The structural framework is a northeast–southwest-trending asymmetric compound syncline. Coal seams commonly dip by 45-70°. The No. 2-1 upper seam and the No. 2-1 seam are the principal seams used in the 2024 coal-loss calculation. The field investigations also documented goafs, faults, surface cracks, disturbed benches, waste accumulations, and fire-related fractures. These features are treated as possible pathways or storage zones for heat and gas, but the present study does not infer a causal contribution from any individual structure without a spatially matched observation.

2.2 Field Investigation and Monitoring

2.2.1 UAV Thermal-Infrared and Ground Surveys

The 2021 field survey used an M300 multirotor equipped with a ZH20T thermal camera. Image acquisition began at approximately 18:00 on 22 April 2021 and continued until before 08:00 on 23 April. The flight height was approximately 238 m, the wind force was 1–3, and 2461 thermal image scenes were acquired. Surface temperature inversion was performed after calibration, but the calibration equation, emissivity setting, atmospheric correction, and temperature uncertainty were not retained in the field dataset. We therefore use the 2021 temperature anomalies as measured field observations and do not re-estimate their absolute temperature values.

The 2021 ground survey followed accessible routes and recorded exposed geological bodies, coal and rock outcrops, cracks, collapse features, waste piles, surface fires, ground-temperature anomalies, water or soil conditions, and nearby power sources. The field dataset contains 41 ground points, consisting of 22 geological points and 19 check points. The point records include location, date, lithology, structure, tectonic information, coal-seam information, temperature, the relation between coal and roof rock, sketches, and photographs. The field program did not use a uniform point spacing or a repeated-measurement design, and the gas sampling interval and instrument model for each ground measurement were not consistently documented.

The 2024 field survey used a DJI Mavic 3T UAV near dawn, approximately from 06:00 to before 08:00 local time, to reduce direct solar heating. The wind condition was below Beaufort force 4 and the flight height was approximately 200 m. Thermal images had a size of 640 × 512 pixels, a spectral range of 8–14 μm, an uncooled VO_x detector, a sensitivity below 50 mK, and a nominal temperature range from −40 to 550 °C. The survey used 80% forward overlap, 70% side overlap, and 8719 thermal images. A C# call to the DJI Thermal SDK and Agisoft Metashape were used to construct the thermal mosaic. Ground-temperature observations were used for temperature-inversion calibration, but the calibration equation and its uncertainty were not retained in the field dataset. Ground validation used an infrared thermometer. The gas analyser, sampling mode, calibration procedure, detection limit, and sampling frequency were not consistently documented. We therefore use gas observations as measured field evidence and do not construct a quantitative gas-emission time series.

The 2024 field dataset contains 52 main field-survey points and a separate set of 29 validation points. Because these point sets were collected for different purposes and their independence cannot be demonstrated, the 52 points are treated as the primary field-observation set and the 29 records are retained as a separate validation category rather than counted as independent replicates.

2.2.2 Boreholes, Geophysical Logging, and Gas Observations

Five verification boreholes were drilled during the 2021 field program, with a total length of 621.66 m. The boreholes were arranged near exploration lines 8, 11, and 15 to constrain the deep-fire extent, burning seams, and temperature anomalies. Drilling was stopped when a fire body or anomalous rock temperature was encountered. The boreholes were not sealed, and markers were installed after drilling. ZK1 was logged. The other boreholes were not logged because of large inclination or fire-safety constraints.

The 2021 logging suite included apparent resistivity, spontaneous potential, natural gamma, density or induced gamma, caliper, deviation, and temperature. The field record

identifies CLGIS1.0 as the interpretation software. The recorded borehole observations include a temperature of approximately 37 degrees C in the coal core and approximately 67 degrees C in the overlying direction together with about 276 ppm CO in ZK2; approximately 64.6 degrees C at about 196 m and a cavity at 197 to 197.5 m in ZK3; approximately 82.3 degrees C at 15 m and about 1000 ppm CO in ZK4; and a borehole-mouth temperature of approximately 82.5 degrees C and about 1000 ppm CO in ZK5. ZK1 showed no clear thermal anomaly. These values are retained as recorded point or interval evidence. They are not converted into a continuous three-dimensional temperature field.

The field dataset also contains gas observations acquired at earlier monitoring dates. The maximum CO concentration was 356 ppm at eight gas points in 2019 and 71 ppm at five points in September 2021. Historical records reported approximately 2 ppm H_2S at selected observation points, whereas the 2024 field descriptions documented pungent H_2S odours without concentration measurements. The dataset does not provide synchronized, repeated measurements of CO_2, O_2, CH_4, gas flux, pressure, or airflow at the same locations and dates. Historical methane values from coal-gas or mine-gas records are therefore not used as contemporaneous indicators of the 2021 or 2024 fire stage.

2.2.3 DInSAR Observations

The DInSAR analysis used Sentinel-1A single-look complex data acquired on 23 September and 16 December 2023. The processing used VV polarization, interferometric wide-swath mode, a 30 m ALOS digital elevation model, ENVI, and SARscape. The temporal baseline was 84 days and the spatial baseline was 110.957 m. The measured deformation range was approximately −0.05 to +0.03 m. These values represent line-of-sight deformation estimates over the 84-day interferometric interval and should not be interpreted as absolute vertical displacement. These products provide short-period deformation context for the 2024 field survey. Because only one interferometric pair was analyzed, the deformation product is not interpreted as a long-term subsidence trend or as evidence that subsurface combustion has ceased.

2.3 Spatial Analysis and Data Processing

The study data were reorganized into a data-audited table with one row for each fire polygon, hot-waste-pile polygon, ground point, borehole observation, gas observation, or DInSAR observation. Each row contains the measurement year, sector, observation type, measured value, unit, spatial identifier, and evidence status. Evidence status is coded as direct observation, interpreted observation, historical value, or accounting scenario. The original Chinese place names, fire-zone identifiers, borehole identifiers, and exploration-line identifiers are retained in the data dictionary so that the English manuscript does not merge distinct entities.

The spatial reference is CGCS2000 with the 1985 national height datum. The 2021 topographic work used GPS or RTK control and recorded maximum engineering survey errors of 0.195 m in the horizontal direction and 0.153 m in elevation. The 2024 survey achieved a free-network photogrammetric bundle-adjustment root-mean-square error of 0.068 m, an image-control-point horizontal error of 0.042 m, and a thermal-mosaic relative offset of less than 0.2 m from the base map. These values describe survey or registration quality. They are not treated as temperature-measurement uncertainties.

The primary spatial unit is the measured fire polygon, hot-waste-pile polygon, ground point, borehole, or DInSAR observation. We do not perform pixel-level fusion, spatial interpolation, kernel smoothing, or three-dimensional inversion because the complete georeferenced raster layers, point coordinates, and uncertainty fields required for those operations were not retained for all measurements. The analysis instead compares whether different evidence types occur within the same measured sector or investigation unit. This preserves the distinction between spatial association and causal control. Surface-area comparisons use square metres. The nominal difference between two recorded areas is calculated as

$$\Delta A = A_2 - A_1 \quad (1)$$

where A_1 and A_2 are the measured areas for the earlier and later surveys, respectively. A percentage change is calculated only when the two values have the same spatial boundary, class definition, and mapping basis. The 2021 detailed fire area of 83,241 m^2 and the 2024 mapped fire-zone area of 81,252.80 m^2 are therefore retained as separate measured values, not as a formally matched change rate, because their survey scopes and classification procedures are not identical. The 2024 hot-waste-pile area of 95,957.27 m^2 is

analyzed as a separate class rather than added to mapped fire-zone area to imply active underground burning.

2.4 Identification of Coal-Fire Evidence Zones

The field dataset does not provide a formal set of temperature, CO, CO_2, O_2, or CH_4 thresholds for dividing the fire into oxidation stages. We therefore do not assign the observations to laboratory-derived low-temperature, accelerated-oxidation, or active-combustion stages. Instead, we use four operational evidence zones that correspond to the measured observation types.

The fire-zone evidence class comprises the 2024 survey units labelled as fire points or fire areas. These units were identified from combined field observations and UAV-based interpretation, but they are not assumed to represent active flaming combustion unless supported by direct evidence such as visible flame, smoke, burned rock, or very high measured temperature. The hot-waste-pile zone consists of the 27 waste-pile units classified separately during the 2024 survey. The subsurface-supported evidence zone consists of borehole intervals or borehole-mouth observations for which elevated temperature, CO, a cavity, or a related combustion interpretation was measured or documented. The unresolved zone includes thermal or field anomalies for which the available measurements do not establish a direct subsurface connection. An unresolved zone is not treated as an extinguished zone.

Evidence strength is described in three levels for interpretation. Level 1 is direct field observation and measurements, such as visible flame, smoke, burned rock, surface cracking, or a measured ground-temperature anomaly. A gas odour is recorded as a qualitative gas indication rather than a quantitative gas measurement. Level 2 is mapped surface thermal evidence without a contemporaneous subsurface measurement. Level 3 is a subsurface constraint from a borehole temperature, CO observation, cavity, or geophysical log. These levels describe evidence type and not fire intensity. They are used to prevent a surface thermal polygon, a hot waste pile, and a borehole observation from being counted as equivalent measurements. The level assignment is an operational rule established for this paper and is not a diagnostic threshold validated by an independent experiment.

2.5 Evaluation of Fire Evolution and Treatment Effectiveness

The available field dataset does not contain a matched, repeated monitoring design before and after a single treatment intervention. It also does not provide treatment dates, treatment volumes, injection pressures, or synchronized post-treatment measurements for every fire zone. The study therefore does not estimate a causal treatment effect. It evaluates fire evolution through a data-constrained comparison of measured evidence: mapped fire-zone area, mapped hot-waste-pile area, the number of anomaly units, open-flame observations, ground-temperature observations, borehole temperature and CO evidence, and the short-period DInSAR deformation range.

The 2021 and 2024 coal-loss estimates are reproduced as accounting scenarios rather than as a validation of fire extinction. The field calculations use the following relations:

$$H = H_1 - H_2 \tag{2}$$

where H is the inferred maximum burning depth, H_1 is the ground elevation, and H_2 is the elevation of the coal-seam floor. The inclined seam area is calculated as

$$S = \frac{S_1}{\cos\theta} \tag{3}$$

where S1 is the mapped horizontal area and theta is the seam dip. Coal loss is then calculated as:

$$Q = S\,m\,p \tag{4}$$

where m is the assumed average coal-seam thickness (m), ϱ is the assumed coal density (t m^{-3}), and Q is the estimated coal loss (t). The equation represents the full-burning scenario used in the field calculation. It does not include a separately measured burning fraction, porosity correction, uncertainty interval, or independent mass-balance check. The 2021 and 2024 values are consequently compared only after their survey boundaries, seam assignments, thicknesses, dip angles, and densities are listed separately. No significance test, predictive model, or causal regression is applied. The reason is that the field dataset contains few time points, nonuniform spatial sampling, no repeated measurements at a common set of points, and no independent untreated control area. This restriction is intentional: a descriptive multi-evidence comparison is more defensible than a statistical treatment claim unsupported by the monitoring design.

2.6 Data Quality and Uncertainty

The main uncertainty sources are spatial sampling, temporal mismatch, measurement documentation, classification consistency, and accounting assumptions. The two field campaigns differ in survey extent, season, UAV platform, thermal acquisition conditions, image-processing workflow, and anomaly-classification scheme. The 2021 dataset contains 41 ground points, whereas the 2024 dataset contains 52 main field-survey points and a separate set of 29 validation points. These counts are reported transparently and are not combined into a single replicate number.

The field dataset provides geometric or image-registration errors for several survey products, but field-temperature accuracy, temperature-inversion residuals, surface emissivity, atmospheric correction parameters, gas-analyser accuracy, gas detection limits, sampling repeatability, and borehole-temperature uncertainty were not consistently documented. These quantities are therefore not invented or propagated into a numerical confidence interval. The UAV detector sensitivity and nominal temperature range are presented as instrument specifications, not as the accuracy of each field temperature.

No unmeasured value is imputed. No smoothing, interpolation, or outlier deletion is applied to the field observations. Values that differ between tables or measurement periods remain flagged as data discrepancies. In particular, the point-count discrepancy, the different measured survey areas, the distinction between active-fire and hot-waste-pile polygons, and the difference between the 2021 and 2024 coal-loss estimates are treated as uncertainties in interpretation. Negative or weak evidence is not converted into evidence of extinction. This rule is essential because a single DInSAR pair or a low surface temperature cannot exclude a deep, spatially disconnected residual heat source.

3. Results

3.1 Spatial Distribution and Classification of High-Temperature Anomalies

The 2024 field survey identified 71 high-temperature anomalies in the Erdaoling mining area based on UAV thermal-infrared imagery, UAV-derived orthophotos, and field validation. These anomalies were classified into 44 fire-zone units and 27 high-temperature gangue-pile units. The fire-zone units occupied a total area of 81,252.80 m², whereas the high-temperature gangue-pile units covered 95,957.27 m². The combined mapped area of the two anomaly classes was therefore 177,210.07 m². The two classes were treated separately because a thermal anomaly within a gangue pile does not necessarily indicate active combustion of an exposed or subsurface coal seam.

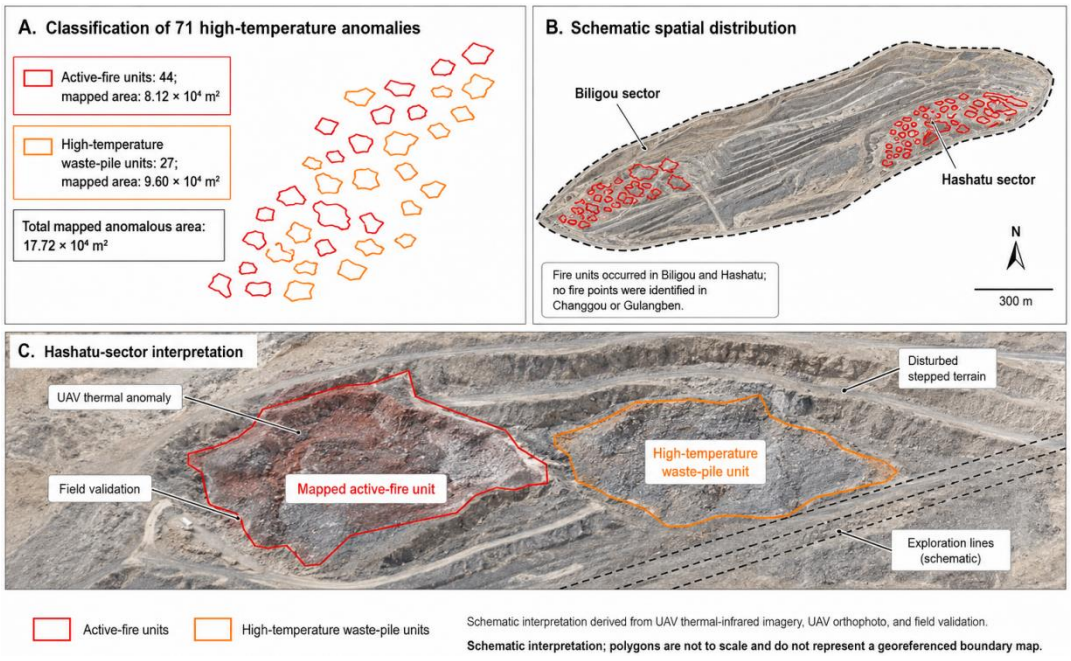


Figure 2. Classification and schematic spatial interpretation of high-temperature anomalies identified from UAV thermal-infrared imagery, UAV-derived orthophotos, and field validation in the Erdaoling

mining area. (A) Classification of 71 anomalies into 44 fire-zone units and 27 high-temperature gangue-pile units. (B) Schematic distribution of fire-zone units in the Biligou and Hashatu sectors. (C) Conceptual interpretation of fire-zone and gangue-pile anomalies in the Hashatu sector. The polygons are schematic and do not represent georeferenced boundaries.

The fire-zone units were concentrated in the Biligou and Hashatu sectors. The Hashatu sector contained 28 fire-zone units, including 26 units within the mining boundary and 2 units outside the boundary. Their total area was 51,814.23 m^2. The Biligou sector contained 16 fire-zone units, including 7 units within the mining boundary and 9 units outside the boundary. Their total area was 29,438.57 m^2. Accordingly, the 44 fire-zone units comprised 33 units within the mining boundaries and 11 units outside the boundaries. Their corresponding areas were 69,384.74 m^2 and 11,868.05 m^2, respectively, consistent with the reported totals of 6.94×10^4 m^2 and 1.18×10^4 m^2. No fire-zone unit was identified in the Changgou or Gulangben sectors during the 2024 survey. As shown schematically in Figure 2, the fire-zone units were generally blocky, discontinuous, and spatially fragmented. The close-up interpretation of the Hashatu sector illustrates how fire-zone anomalies were distinguished from thermally anomalous gangue piles using the combined evidence from thermal imagery, orthophotos, and field observations. Because Figure 2 is a schematic interpretation rather than a georeferenced boundary map, the illustrated polygons are intended to represent anomaly types and their spatial relationships, not the exact geometry or area of individual fire zones. The 2024 fire-zone distribution broadly overlapped the area investigated in the earlier survey. For the broader exploration-line 8–19 comparison reported in the survey, the 2021 fire area was approximately 1.213×10^5 m^2, compared with 8.12×10^4 m^2 in 2024. This yielded a nominal difference of approximately 4.01×10^4 m^2, or 33.06%. The narrower 2021 detailed area of 83,241 m^2 was not used to calculate this percentage because it represents a different investigation scope. This comparison should be interpreted cautiously because the two surveys differed in survey extent, polygon delineation, classification criteria, and interpretation procedures. In particular, the 2024 dataset separately identified high-temperature gangue piles, whereas these features were not necessarily treated as a separate category in the earlier survey. Therefore, the comparison indicates a broad reduction in delineated fire-zone area rather than a strictly matched measurement of fire decay.

The mapped fire zones occur within a strongly disturbed mining landscape containing steeply dipping coal seams, historical workings, goafs, excavation pits, stepped slopes, waste platforms, faults, and surface cracks. Field interpretations associated the Biligou fire mainly with the No. 2-1 coal seam. In the Hashatu sector, the 2021 detailed interpretation associated the fire with the upper No. 2-1 seam, whereas the 2024 field observations suggested that the two open-fire points near exploration line 15 may involve both the upper No. 2-1 seam and the No. 2-1 seam. The field investigation also described spatial associations between fire distribution, coal-seam strike and dip, and different types of fractures, including structural, gravity-related, and fire-induced fractures. The reported fracture dips were approximately 75-80°. These observations support a spatial association between the fire zones and disturbed geological–mining structures, but they do not by themselves demonstrate that a specific fault, goaf, or fracture caused the initiation or expansion of an individual fire zone. The results presented here are based on the 2024 fire-zone and high-temperature gangue-pile measurements, the corresponding UAV interpretation products, field validation records, and the 2021 investigation data used for comparison. The identification of fragmented fire zones, their broad spatial consistency with the earlier investigation, and the possible role of fractures as preferential pathways should therefore be understood as field-based interpretations or cautious inferences rather than independently tested causal relationships.

3.2 Field Evidence Supporting the Interpretation of Thermally Anomalous and Fire-Affected Areas



Figure 3. Field observations supporting the interpretation of thermally anomalous and fire-affected areas. (A) Historical open-flame conditions documented during the 2021 investigation. (B) Smoking high-temperature gangue pile. (C) Incandescent fragments in fire-affected waste material. (D) Surface cracking. (E) In situ temperature measurement. (F) Smoke or steam emission from a high-temperature waste pile.

Field observations provided independent, point-based support for the interpretation of thermally anomalous and fire-affected areas derived from the UAV remote-sensing data. Figure 3 combines historical and recent field evidence, including historical open flames, smoking gangue piles, incandescent fragments, surface cracking, in situ temperature measurements, and smoke or steam emission from thermally anomalous waste materials. Panel A shows historical open-flame conditions documented during the 2021 detailed investigation, whereas Panels B-F present representative field observations from the 2024 survey. These observations demonstrate that the thermal anomalies were associated with different physical manifestations, ranging from visible combustion to residual heat retained in gangue piles and disturbed mine surfaces. The temperature and gas observations summarized in Table 1 were collected at fire points, gangue piles, smoking locations, boreholes, and relatively unaffected surfaces. Because these measurements were obtained at discrete locations and under different field conditions, they represent local thermal and gas contrasts rather than a statistically sampled temperature or gas-concentration field. The distinction between direct measurements and qualitative field observations is therefore important when interpreting the remote-sensing results. The historical field records provide clear evidence of strong thermal activity. The 2021 investigation reported fire-zone surface temperatures of 40–165 °C and flame temperatures of 630-800 °C (Table 1; Figure 3A). During the 2024 survey, two open-fire points, Fire-13 and Fire-17, were identified near exploration line 15. Their surface temperatures exceeded 380 °C, and both sites showed visible smoke, burned-rock characteristics, and a pungent hydrogen-sulfide odour. These observations are consistent with the open-fire and fire-affected materials illustrated in Figure 3A and Figure 3C. Because no H_2S concentration was measured at these locations, the odour observations are treated as qualitative evidence of gas release rather than quantitative gas measurements.

The 2024 field photographs also document thermally anomalous materials without visible open flames. Figure 3B shows a smoking high-temperature gangue pile, whereas Figure 3C shows incandescent fragments within fire-affected waste material. At DC2, a high-temperature fire-slag point showed a temperature of 22.6 °C, slight white steam, and no visible flame. DC3, a high-temperature gangue pile, showed a temperature of 24.9 °C together with a wet surface and slight steam emission. At DC49, a high-temperature smoke point also showed a temperature of 24.9 °C and local white steam emission. DC52, located

outside the mining boundary, recorded 36.5 °C at a gangue pile with abundant white smoke and a pungent H2S odour. These observations correspond to the smoking waste-pile and gas- or steam-emission features illustrated in Figure 3B and Figure 3F. They indicate that thermally anomalous gangue piles may retain heat or release steam and gases even when visible open combustion is absent. Surface deformation and cracking provide additional contextual evidence. Figure 3D shows a surface crack developed in disturbed mine ground. Such cracks may reflect gravity-driven deformation, mining disturbance, or thermal effects. They may also provide preferential pathways for heat and gas migration. However, the photograph alone does not establish the origin of an individual crack or demonstrate a direct causal relationship between cracking and fire-zone expansion. Figure 3E illustrates the field temperature-check procedure used to validate the remote-sensing interpretation. The measurements were therefore used as point-based validation data rather than as a continuous temperature map. The 2024 validation records also showed clear local temperature contrasts between thermally anomalous materials and relatively cool surfaces (Table 1). The temperature was 0.5 °C at a vegetated point in Changgou and -11.0 °C at an exposed bedrock surface near a mining road. These values were substantially lower than the temperatures measured at the two open-fire points and at the high-temperature gangue-pile and smoking points. The contrast supports the discrimination of fire-affected or thermally anomalous materials from ordinary or relatively cool surfaces. Nevertheless, the values should not be interpreted as representative temperatures for entire land-cover or geological categories. Additional evidence was obtained from historical gas records and borehole observations (Table 1). The 2019 observations reported a maximum CO concentration of approximately 356 ppm at eight gas-observation points and an H_2S concentration of approximately 2 ppm. The September 2021 observations reported a maximum CO concentration of approximately 71 ppm at five points. At borehole ZK2, a CO concentration of approximately 276 ppm was reported together with a coal-core temperature of approximately 37 °C and a rock temperature of approximately 67 °C toward the surface. ZK4 showed a reported CO concentration of approximately 1000 ppm and a temperature of approximately 82.3 °C at a depth of 15 m, whereas ZK5 showed a similar CO concentration and a borehole-mouth temperature of approximately 82.5 °C. At ZK3, a temperature of approximately 64.6 °C was recorded at approximately 196 m depth, together with a cavity at 197-197.5 m; however, no corresponding CO concentration was available. ZK1 showed no clear thermal anomaly.

The gas observations should be interpreted cautiously because the records were obtained at different locations and under different observation conditions. The CO maxima reported for 2019 and 2021 cannot be treated as repeated measurements at identical monitoring points. The available records also do not provide spatially matched measurements of CO_2, O_2, or CH_4 during the 2021 and 2024 fire surveys. Historical coal-gas records reported average CH_4 contents of 79.82-92.46% in samples from six boreholes, but these values describe coal-gas or mine-gas compositions rather than contemporaneous concentrations in fire-related surface emissions. Taken together, the photographic observations in Figure 3 and the quantitative records in Table 1 support a qualitative association among elevated temperature, CO occurrence, H_2S indications, smoke, incandescent fragments, cavities, open flames, burned rock, and surface cracking. The co-occurrence of these indicators supports the interpretation that at least some of the remote-sensing anomalies correspond to residual combustion or heat-retaining fire-affected materials. However, the available evidence does not establish a continuous multi-gas concentration field, a gas-ratio classification of combustion stages, or a quantitative relationship between gas concentration and fire intensity. Estimates of CO_2 production or release derived from coal-loss and gas-balance calculations were therefore not treated as direct gas measurements or used to construct spatial gas distributions.

Table 1. Selected field temperature and gas observations used to support the interpretation of thermally anomalous and fire-affected areas

Year	Location or observation	Measured field evidence	Interpretation

	point		
2021	Fire-zone surfaces	Surface temperature: 40–165 °C	Elevated temperature in fire-affected areas
2021	Historical open-flame areas	Flame temperature: 630–800 °C; visible open flame	Strong evidence of historical surface combustion
2024	Fire-13 and Fire-17 near exploration line 15	Surface temperature: >380 °C; smoke, burned rock, and pungent H2S odour	Documented open-fire points with strong thermal and combustion-related field evidence
2024	DC2, high-temperature coal-slag point	22.6 °C; slight white steam; no visible flame	Localized thermal anomaly or residual heat
2024	DC3, high-temperature gangue pile	24.9 °C; wet surface and slight white steam; no visible flame	Thermally anomalous gangue pile without visible open combustion
2024	DC49, high-temperature smoke point	24.9 °C; white steam and wet surface	Localised smoke or heat-release point
2024	DC52, gangue pile outside the mining boundary	36.5 °C; abundant white smoke and pungent H2S odour	High-temperature gangue pile with qualitative evidence of gas release
2024	DC40, vegetated surface in Changgou	0.5 °C; no gas or smoke observed	Reference surface without an evident thermal anomaly
2024	DC50, exposed bedrock near a mining road	−11.0 °C; no gas or smoke observed	Relatively cool ordinary surface
2019	Eight historical gas-observation points	Maximum CO: approximately 356 ppm; H2S: approximately 2 ppm	Historical evidence of harmful-gas occurrence
2021	Borehole ZK2	Coal-core temperature: approximately 37 °C; rock temperature toward the surface: approximately 67 °C; CO: approximately 276 ppm	Borehole thermal and gas anomaly
2021	Borehole ZK4 at 15 m depth	Temperature: approximately 82.3 °C; CO: approximately 1000 ppm	Strong borehole thermal and CO anomaly
2021	Borehole ZK5	Borehole-mouth temperature: approximately 82.5 °C; CO: approximately 1000 ppm	Strong borehole thermal and CO anomaly
2021	Borehole ZK3 at approximately 196–197.5 m depth	Temperature: approximately 64.6 °C at approximately 196 m; cavity at 197–197.5 m; CO value unavailable	Thermal anomaly associated with a subsurface cavity
2021	Borehole ZK1	No clear thermal anomaly; no corresponding gas anomaly reported	No clear borehole anomaly

3.3 Temporal Evolution of the Fire Zone

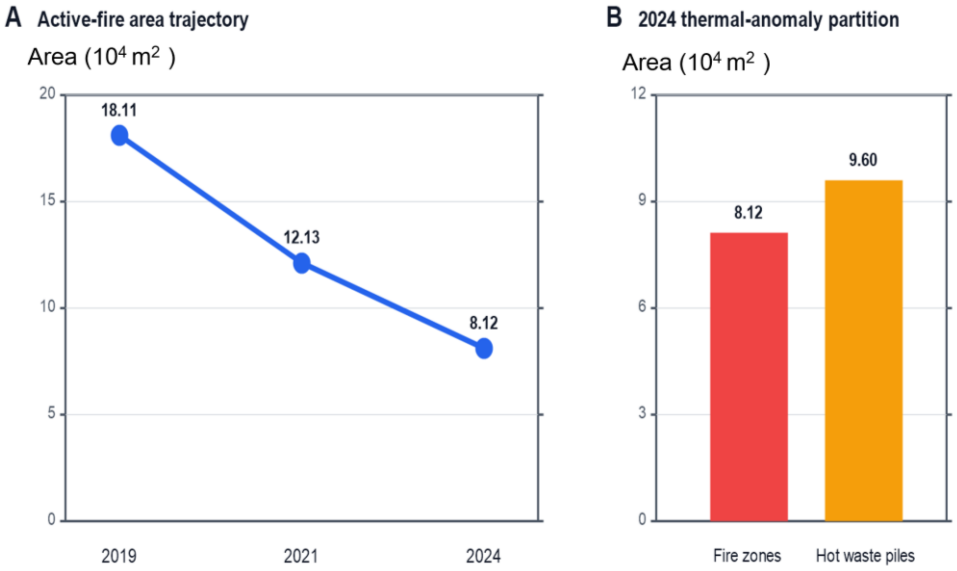


Figure 4. Reported fire-zone and thermal-anomaly areas across different survey periods. Panel A summarizes the recorded area values from 2019 to 2024, whereas Panel B separates the 2024 high-temperature anomaly footprint into fire-zone units and high-temperature gangue-pile units.

The dataset includes survey products from 2007–2012, 2019, April and September 2021, September–December 2023, and January 2024 (Table 2). Because these products differ in spatial coverage, acquisition method, classification scheme, and observation design, they are used for descriptive comparison rather than as a harmonized time series. But it does not form a single harmonized time series at fixed boundaries and fixed monitoring points. The temporal results are therefore presented as measurement-period-specific observations rather than as a continuous fire-growth curve. The historical measurements show different fire areas for different survey products. The 2007 detailed field investigation measured 85.99 × 10^4 m^2 for four Gulangben fire zones and a combustion depth of 50–360 m measured along the seam dip direction. The 2012 airborne thermal survey measured a coal-fire area of 12.29 × 10^4 m^2 and an open-flame area of 3573.93 m^2. The 2019 remote-sensing survey measured a thermal-anomaly area of 42.89 × 10^4 m^2, a coal-fire area of 18.11 × 10^4 m^2, and an open-flame area of 1298.85 m^2. The September 2021 remote-sensing survey measured a coal-fire area of 12.13 × 10^4 m^2 and an open-flame area of 1142.3 m^2. Within this measurement-period comparison, both reported area measures were lower in September 2021 than in 2019. The comparison remains descriptive because the field dataset does not provide complete polygon-level harmonization and repeated-point measurements needed for a formal trend analysis. The April 2021 detailed field investigation measured 83,241 m^2 for the fire area along exploration lines 8–16. The January 2024 field survey measured 81,252.80 m^2 for 44 fire units and identified 27 hot-waste-pile units covering 95,957.27 m^2. The 2024 field measurements place the fire positions broadly within the 2021 investigation area but resolve the distribution as more fragmented. Because the 2021 detailed survey and the 2024 UAV survey have different survey boundaries and classification schemes, their measured areas are not converted into a formal percentage change in this study. The gas records also contain dated maxima. The recorded maximum CO decreases from 356 ppm at eight points in 2019 to 71 ppm at five points in September 2021. The later 2021 borehole measurements include approximately 276 ppm at ZK2 and approximately 1000 ppm at ZK4 and ZK5. These observations do not establish a monotonic temporal decrease or increase because the boreholes, gas points, sampling settings, and observation contexts are different. Temperature records are likewise not repeated at a common set of locations. The 2023 September to December DInSAR result is a single 84-day interferometric observation and does not provide a long-term deformation time series. The analysis uses the dated area and gas records summarized in Table 2 and the spatial comparison shown in Figure 4. The evidence supports field-record-level differences between dated surveys. It does not support a continuous

rate of fire migration, a statistically tested decline in temperature, or a monotonic trend in CO concentration. Statements that the fire system decreased or fragmented are retained as field-record descriptions and are not presented as causal estimates of treatment performance.

Table 2. Summary of dated survey products and their comparability with the January 2024 investigation

Survey period	Survey product	Main reported result	Comparability with January 2024
2007–2012	Historical field and airborne thermal surveys	2007: four Gulangben fire zones, 85.99 × 10^4 m^2; 2012: coal-fire area 12.29 × 10^4 m^2 and open-flame area 3573.93 m^2	Low; historical boundaries and classification procedures differ
2019	Remote-sensing survey	Thermal-anomaly area 42.89 × 10^4 m^2; coal-fire area 18.11 × 10^4 m^2; open-flame area 1298.85 m^2	Low to moderate; survey extent and classification differ
Apr-21	Detailed field survey; 5.1013 km^2 along exploration lines 8–16	Fire area 83,241 m^2, including Biligou, Hashatu, and the area outside the Biligou mining boundary	Moderate for spatial context; not directly interchangeable
Sep-21	Remote-sensing survey	Coal-fire area 12.13 × 10^4 m^2; open-flame area 1142.3 m^2	Moderate for descriptive comparison only
September–December 2023	Sentinel-1A DInSAR; one interferometric pair	84-day interferometric observation; deformation range approximately −0.05 to +0.03 m	Complementary but non-equivalent evidence
Jan-24	UAV thermal-infrared survey and field investigation; approximately 10.63 km^2	44 fire-zone units covering 81,252.80 m^2; 27 high-temperature gangue-pile units covering 95,957.27 m^2	Reference dataset for the present study

3.4 Relationships Among Geological Structures, Temperature, and Gas Indicators

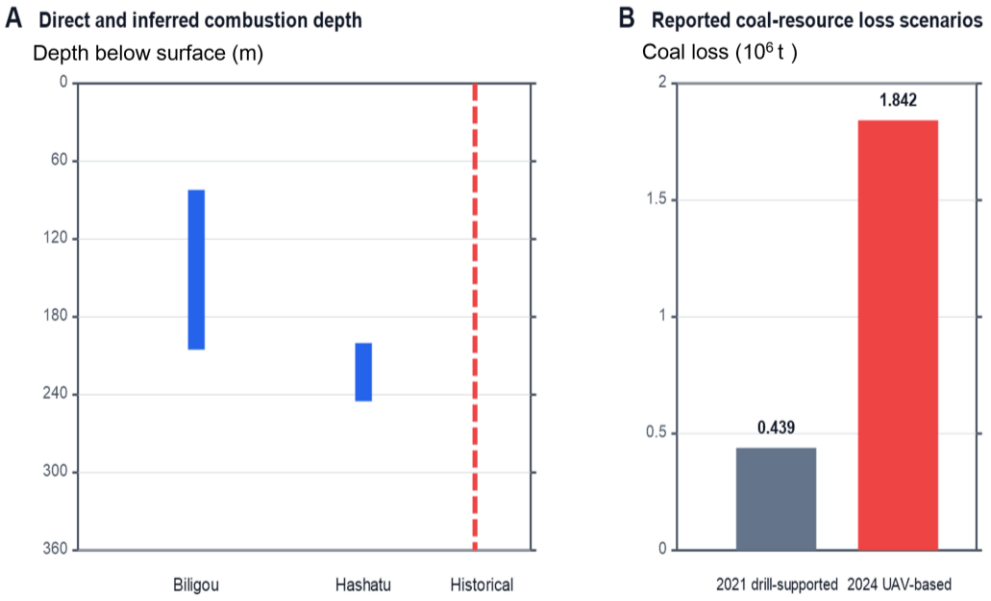


Figure 5. Subsurface and accounting evidence. Panel A separates drill-supported combustion depths

from the historically inferred upper-bound depth. Panel B shows why the 2021 and 2024 coal-loss estimates should be treated as scenarios until their calculation boundaries are reconstructed.

The recorded spatial relationship is strongest for coal-seam geometry and fractures, but the available data do not establish a structure-specific causal effect. The field investigations describe fire distribution along coal-seam strike and dip and identify structural, gravity-related, and fire-induced fractures as the main fracture classes. The recorded average fracture dip is 75 to 80 degrees. The 2021 and 2024 maps also show fire units in a landscape affected by old workings, goafs, excavation pits, stepped slopes, and waste platforms. The borehole measurements provide local depth constraints that are consistent with subsurface thermal or combustion anomalies. ZK3 contains a high-temperature interval at approximately 196 m and a cavity immediately below it. ZK4 and ZK5 contain high-temperature and CO observations. These boreholes were part of the 2021 detailed field investigation, but the available measurements do not provide a complete coordinate-based overlay between every borehole, every fracture, every goaf polygon, and every 2024 thermal unit. We therefore report co-occurrence at the investigation-unit level rather than calculating a distance-dependent structure effect. The 2017 goaf record identifies goafs above the +1800 m level in eight coal seams and records a total goaf area of approximately 640 × 10^4 m^2 for the relevant exploration-line area. This large disturbed subsurface environment overlaps the general mining setting, but the available data do not quantify the intersection between the goaf polygons and the 2024 fire polygons. Similarly, the measured fracture types and dips are not accompanied by permeability, pressure, airflow, or oxygen-concentration measurements. The results therefore support a spatial association between residual fire evidence and a structurally disturbed coalfield. They do not demonstrate that a particular fault or fracture caused fire propagation.

Evidence audit. The analysis uses the 2021 detailed geological map, the 2017 goaf summary, the 2024 fire-distribution map, and the borehole measurements in Table 1. The corresponding manuscript items are Figure 4, and 6. The phrase "structure-controlled" would exceed the evidence available here. The defensible wording is "spatially associated with coal-seam geometry and fractured or mined ground."

3.5 Identification of Different Combustion or Risk Zones

The multi-source field data support four evidence-based zones rather than a laboratory-defined sequence of oxidation stages. The first zone is the mapped active-fire zone. It contains the 44 fire units identified in 2024, covers 81,252.80 m^2, and includes two open-fire points with surface temperatures above 380 °C, smoke, burned rock, and pungent H_2S odour. The Biligou and Hashatu sectors contain all 2024 fire units identified in the study. The second zone is the hot-waste-pile zone. It contains 27 units covering 95,957.27 m^2. The field measurements include surface temperatures of 24.9-82.6 °C at representative hot-waste-pile points, together with steam or smoke descriptions at some locations. These units are classified separately because the measurements do not prove that the heat originates from an actively burning underground coal seam. The third zone is the subsurface-supported evidence zone. It includes the borehole observations at ZK2, ZK3, ZK4, and ZK5. The evidence consists of elevated temperature, CO, or a cavity at depth. ZK1 is retained as a no-clear-anomaly observation. These borehole observations constrain the possibility of residual subsurface heat but do not define a continuous underground fire boundary. The fourth zone is the unresolved zone. It includes thermal or field observations for which the available measurements do not provide a direct subsurface measurement or a complete gas record. Areas without a measured thermal or field anomaly are not classified as extinguished because the available observations are spatially incomplete and a single surface survey cannot exclude a deeper, disconnected heat source. Evidence audit. The zone boundaries follow the measured fire polygons, hot-waste-pile polygons, borehole identifiers, and field-validation records. The corresponding manuscript items are Figure 4, 5, and 6 and Tables 1 and 2. The four-zone scheme is an operational classification created for this paper. It is not a validated fire-intensity scale and should not be described as a chemical-stage model.

3.6 Response to Fire-Control Measures

The field dataset documents fire-control and goaf-treatment activities and records lower fire-

area or CO maxima in some later surveys, but it does not provide a matched treatment experiment. The 2019 survey was conducted during the period of goaf treatment and identified new fire sources in treatment areas. The September 2021 remote-sensing summary records the disappearance of fire points 19, 20, 21, and 25 after treatment, a decrease in measured coal-fire area from 18.11×10^4 to 12.13×10^4 m², and a change in open-flame area from 1298.85 to 1142.3 m². The same summary records a lower maximum CO value in September 2021 than in 2019. These are field-record-level before-and-after observations, not a causal estimate, because treatment intensity, exact treatment timing, untreated control areas, and repeated measurements at common points are not provided. The 2024 investigation still identifies 44 fire units, 27 hot-waste-pile units, two open-fire points, smoke or odour observations, and borehole-supported residual thermal or gas evidence inherited from the 2021 investigation. Thus, the available data show that the mapped surface fire system changed after years of treatment and that residual thermal evidence remained. They do not support a numerical treatment efficiency, a complete extinction claim, or a causal attribution of each spatial change to a specific remediation measure. Evidence audit. The analysis uses the historical treatment chronology, the 2019 and September 2021 remote-sensing measurements, and the 2024 fire and hot-waste-pile measurements. The corresponding manuscript items are Figure 4, Figure 6, and Table 2. The treatment response is described only as "observed after treatment" or "consistent with a reduction in mapped surface fire area." The data do not support the statement that treatment caused each spatial change without matched spatial and temporal monitoring.

4. Discussion

4.1 Surface-Area Contraction Is Not Equivalent to Subsurface Extinction

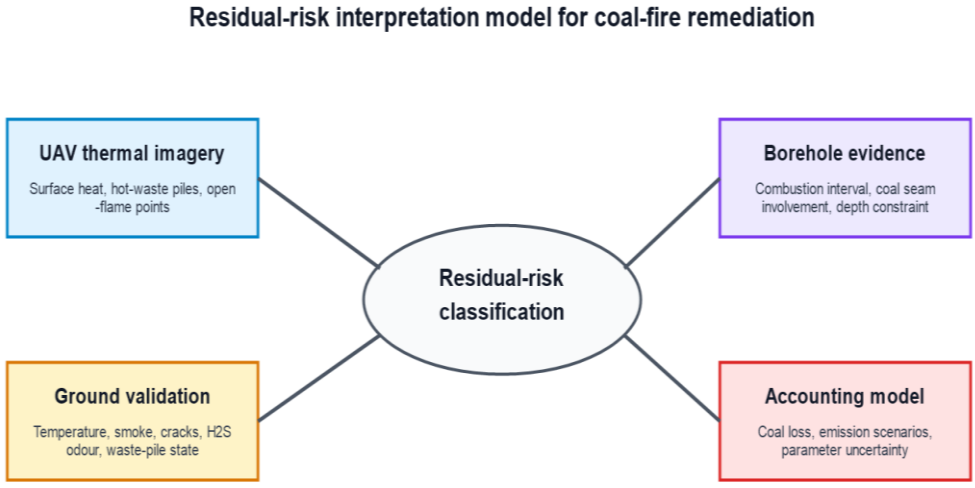


Figure 6. Conceptual model for post-remediation residual-risk classification. The model treats UAV thermal evidence, ground observations, borehole constraints, and accounting scenarios as linked but non-equivalent evidence classes.

The central result is the coexistence of a smaller or more fragmented mapped fire system with independent residual indicators. The 2024 survey records 81,252.80 m² of fire units and 95,957.27 m² of hot-waste-pile units. It also records two open-fire points above 380 °C, field smoke and odour, and 2021 borehole observations with temperatures of approximately 64.6 to 82.5 °C or CO concentrations of approximately 276 to 1000 ppm. These observations do not prove that every hot surface unit is connected to a deep coal fire. They do show that a decrease in a mapped surface-fire class cannot, by itself, establish subsurface extinction. The apparent surface and subsurface mismatch has two evidence-based components. First, hot waste piles form a separate and larger mapped area than the active-fire class in 2024. Heat in a waste pile can therefore contribute to the surface thermal signal without representing the same source as a burning seam. Second, the borehole constraints are sparse and temporally different from the 2024

UAV survey. A surface polygon and a borehole anomaly cannot be assumed to be vertically coupled without a spatially matched subsurface model. The appropriate conclusion is therefore one of residual-evidence coexistence, not a quantified decoupling coefficient.

4.2 Geological Structures Provide a Plausible Pathway Framework, Not a Demonstrated Propagation Law

The spatial association with steep coal seams, mined ground, goafs, and fractures is consistent with a coupled heat and gas pathway framework. Coal-seam strike and dip provide a geometric direction for elongated fire development, while open workings, collapse zones, and fractures can connect shallow and deeper voids. The recorded fracture dips of 75 to 80 degrees and the field occurrence of cracks, steam, smoke, and hot waste material are compatible with such connectivity.

The data do not measure oxygen flux, permeability, pressure difference, fracture aperture, or airflow along any identified structure. They therefore cannot distinguish whether a fracture supplied oxygen, transported heat, released gas, or simply formed after heating. The interpretation that heat spreads mainly along fractures is scientifically plausible, but it remains a hypothesis for this dataset. A causal structure-control claim would require common-coordinate overlays, repeated gas and temperature measurements, and a flow or heat-transfer model.

4.3 CO Is Useful as Local Evidence, but the Available Gas Record Cannot Define Combustion Stages

The CO observations provide local support for residual fire evidence at selected boreholes and historical observation points. The combination of CO with temperature or a cavity at ZK2, ZK4, and ZK5 is stronger than a temperature anomaly alone. However, the record contains maxima from different point sets and dates. The 2019 maximum of 356 ppm, the September 2021 maximum of 71 ppm, and the approximately 1000 ppm values at ZK4 and ZK5 cannot be arranged into a single temporal trajectory.

The absence of synchronized CO_2, O_2, CH_4, gas-flux, and pressure data prevents a quantitative gas-ratio diagnosis. The recorded CH_4 range of 79.82 to 92.46 percent describes historical coal gas, not a contemporaneous fire plume. The recorded CO_2 values are calculation outputs rather than direct field concentrations or fluxes. Consequently, the present study can identify gas-supported evidence units, but it cannot assign low-temperature oxidation, accelerated oxidation, active combustion, or decay stages from the available gas data.

4.4 Weak DInSAR Deformation Does Not Resolve the Thermal State of the Subsurface

The DInSAR result covers an 84-day interval from September to December 2023 and records deformation between −0.05 and +0.03 m. The measurements show most of the area as stable, with local increases in surface elevation in parts of Biligou and Changgou and a general lowering tendency in much of Hashatu. This result constrains short-period surface deformation. It does not measure temperature, gas concentration, oxygen supply, or combustion rate. Residual combustion can remain spatially disconnected from the deformation field, and a single interferometric pair cannot establish whether a weak deformation signal reflects a stable thermal source, a cooled zone, a rigid overburden, or a short observation window. The defensible interpretation is that the measured deformation field does not exclude residual coal-fire evidence identified by thermal, field, gas, or borehole observations.

4.5 What Can and Cannot Be Concluded About Treatment Effectiveness

The dated remote-sensing measurements are consistent with a reduction in some surface-fire indicators after treatment. The disappearance of four named fire points, the lower measured coal-fire area in the September 2021 summary, and the lower measured CO maximum provide field evidence of change. The 2024 survey, however, records continuing fire units, hot-waste piles, open flame, and subsurface-supported anomalies. The two statements can coexist because they refer to different evidence classes and because surface classification does not measure the full underground system.

The field dataset cannot estimate treatment efficiency as a percentage of extinguished underground fire, nor can it identify which treatment method produced a particular change. The results support a monitoring criterion based on repeated agreement among surface thermal mapping, field temperature and gas observations, borehole evidence, and deformation records. This is a measurement requirement derived from the evidence structure, not a measured treatment outcome.

4.6 Data Limitations and the Scope of Inference

The strongest limitations are the lack of common-coordinate raw layers, the absence of repeated measurements at fixed points, inconsistent survey boundaries, incomplete gas documentation, and the absence of a control area. The 2021 and 2024 area estimates also use different investigation scopes and classification schemes. The difference between the 2021 detailed coal-loss estimate of 43.9×10^4 t and the 2024 estimate of 184.19×10^4 t therefore represents different accounting scenarios rather than a measured fourfold change in resource loss.

Within these limits, the study supports three restrained conclusions. The 2024 survey identifies a spatially fragmented surface thermal-risk system. The field and borehole records show that residual high-temperature or gas-associated evidence remains at selected locations. The field dataset does not justify treating surface-area contraction, low deformation, or a lower maximum CO value as independent proof of underground extinction. These conclusions are directly tied to the recorded data and remain transferable only to coal-fire settings with comparable differences between surface observations and sparse subsurface constraints.

5. Conclusions

Taken together, five conclusions are supported by the field measurements. First, the 2024 survey identifies a fragmented and discontinuous thermal-risk system in the Biligou and Hashatu sectors, with 44 fire units covering 81,252.80 m^2 and 27 hot-waste-pile units covering 95,957.27 m^2; the 2021 and 2024 areas are not directly converted into a decay rate because their survey extents and classification procedures differ. Second, the fire distribution is spatially associated with coal-seam geometry, mined ground, goafs, and fractured zones, including measured fracture dips of approximately 75–80°, but the available data do not prove a causal effect of any single structure. Third, surface temperatures of 40–165 °C in 2021, flame temperatures of 630–800 °C, 2024 open-fire temperatures above 380 °C, borehole temperatures of approximately 64.6–82.5 °C, and CO values of approximately 276–1000 ppm provide local evidence of residual thermal or gas activity, but the incomplete and non-synchronous CO_2, O_2, and CH_4 records cannot define a complete combustion-stage sequence. Fourth, surface fire polygons, hot-waste piles, field temperature and gas observations, borehole anomalies, and DInSAR deformation should be treated as complementary but non-equivalent evidence because surface-area change or weak deformation alone cannot demonstrate subsurface extinction. Finally, the interpretation remains limited by inconsistent survey boundaries, sparse repeated measurements, incomplete gas monitoring, and the lack of a long-term deformation series. Future work should combine repeated observations at fixed coordinates with unified fire boundaries, long-term DInSAR monitoring, and coupled heat-transfer and gas-flow modeling.

Author Contributions

Conceptualization, J.L.; methodology, J.L.; investigation, S.Z. and R.H; writing-review and editing, X.Z.; Y.X. All authors have read and agreed to the published version of the manuscript.

Declaration of Competing Interest

The authors declare no competing financial interest.

Acknowledgment

The authors gratefully acknowledge the support and resources provided by Inner Mongolia Taixi Coal Group Co., Ltd. during the course of this research.

References

Agarwal R, Singh D, Chauhan D S, et al. (2006). Detection of coal mine fires in the Jharia coal field using NOAA/AVHRR data. *Journal of Geophysics and Engineering, 3*(3), 212-218.

Carras J N, Day S J, Saghafi A, et al. (2008). Greenhouse gas emissions from low-temperature oxidation and spontaneous combustion at open-cut coal mines in Australia. *Geomorphology, 78*(2), 161-168.

Carras J N, Young B C. (1994). Self-heating of coal and related materials: Models, application and test methods. *Progress in Energy and Combustion Science, 20*(1), 1-15.

Chatterjee R S. (2006). Coal fire mapping from satellite thermal IR data – a case example in Jharia Coalfield, Jharkhand, India. *ISPRS Journal of Photogrammetry and Remote Sensing, 60*(2), 113-128.

Kuenzer C, Bachmann M, Mueller A, et al. (2008). Partial unmixing as a tool for single surface class detection and time series analysis. *International Journal of Remote Sensing, 29*(11),

3233-3255.

Kuenzer C, Hecker C, Zhang J, et al. (2008). The potential of multidiurnal MODIS thermal band data for coal fire detection. *International Journal of Remote Sensing, 29*(3), 923-944.

Kuenzer C, Stracher G B. (2012). Geomorphology of coal seam fires. *Geomorphology, 138*(1), 209-222.

Kuenzer C, Zhang J, Li J, et al. (2007). Detecting unknown coal fires: synergy of automated coal fire risk area delineation and improved thermal anomaly extraction. *International Journal of Remote Sensing, 28*(20), 4561-4585.

Kuenzer C, Zhang J, Tetzlaff A, et al. (2007). Uncontrolled coal fires and their environmental impacts: Investigating two arid mining regions in north-central China. *Applied Geography, 27*(1), 42-62.

Liang Y, Yang Y, Guo S, et al. (2023). Combustion mechanism and control approaches of underground coal fires: a review. *International Journal of Coal Science & Technology, 10*(1), 24.

Liang Y, Yang Y, Guo S, et al. (2023). Combustion mechanism and control approaches of underground coal fires: a review. *International Journal of Coal Science & Technology, 10*(1), 24.

Lu X, Deng J, Xiao Y, et al. (2022). Recent progress and perspective on thermal-kinetic, heat and mass transportation of coal spontaneous combustion hazard. *Fuel, 308*, 121234.

Onifade M, Genc B. (2020). A review of research on spontaneous combustion of coal. *International Journal of Mining Science and Technology, 30*(3), 303-311.

Onifade M. (2022). Countermeasures against coal spontaneous combustion: a review. *International Journal of Coal Preparation and Utilization, 42*(10), 2953-2975.

Prakash A, Gupta R P. (1999). Surface fires in Jharia coalfield, India-their distribution and estimation of area and temperature from TM data. *International Journal of Remote Sensing, 20*(10), 1935-1946.

Qingwei Li, Yang Xiao, Kaiqi Zhong, et al. (2020). Overview of commonly used materials for coal spontaneous combustion prevention. *Fuel, 275*, 117981.

Raju A, Mehdi K. (2023). SBAS-InSAR analysis of regional ground deformation accompanying coal fires in Jharia Coalfield, India. *Geocarto International, 38*(1), 2167004.

Shao Z, Li Y, Deng R, et al. (2021). Three-dimensional-imaging thermal surfaces of coal fires based on UAV thermal infrared data. *International Journal of Remote Sensing, 42*(2), 672-692.

Song Z, Huang X, Jiang J, et al. (2020). A laboratory approach to CO_2 and CO emission factors from underground coal fires. *International Journal of Coal Geology, 219*, 103382.

Song Z, Huang X, Kuenzer C, et al. (2020). Chimney effect induced by smoldering fire in a U-shaped porous channel: A governing mechanism of the persistent underground coal fires. *Process Safety and Environment Protection, 136*, 136-147.

Song Z, Kuenzer C. (2014). Coal fires in China over the last decade: A comprehensive review. *International Journal of Coal Geology, 133*, 72-99.

Stracher G B, Taylor T P. (2004). Coal fires burning out of control around the world: thermodynamic recipe for environmental catastrophe. *International Journal of Coal Geology, 59*(1), 7-17.

Turner D, Lucieer A, Malenovský Z, et al. (2014). Spatial co-registration of ultra-high resolution visible, multispectral and thermal images acquired with a Micro-UAV over antarctic moss beds. *Remote Sensing, 6*(5), 4003-4024.

Wang T, Wang H, Fang X, et al. (2023). Research progress and visualization of underground coal fire detection methods. *Environmental Science and Pollution Research, 30*(30), 74671-74690.

Wang T, Wang Y, Zhao F, et al. (2022). A spatio-temporal temperature-based thresholding algorithm for underground coal fire detection with satellite thermal infrared and radar remote sensing. *International Journal of Applied Earth Observation and Geoinformation, 110*, 102805.

Zhang X, Zhang J, Kuenzer C, et al. (2004). Capability evaluation of 3-5 μm and 8-12.5 μm airborne thermal data for underground coal fire detection. *International Journal of Remote Sensing, 25*, 2245-2258.

Zhang Y, Wang J, Wu J, et al. (2015). Modes and

kinetics of CO_2 and CO production from low-temperature oxidation of coal. *International Journal of Coal Geology*, *140*, 1-8.

Zhou C, Zhang Y, Wang J, et al. (2017). Study on the relationship between microscopic functional group and coal mass changes during low-temperature oxidation of coal. *International Journal of Coal Geology*, *171*, 212-222.